Available online at www.sciencedirect.com
ScienceDirect
Acta Materialia 55 (2007) 4817–4822
Acta MATERIALIA
www.elsevier.com/locate/actamat

The influence of lattice strain on pearlite formation in Fe–C

I. Steinbach *, M. Apel

RWTH-Aachen, Access e.V., Intzestrasse 5, 52072 Aachen, Germany

Received 31 January 2007; received in revised form 15 March 2007; accepted 1 May 2007
Available online 28 June 2007

Abstract

The effect of stress and strain on the transformation kinetics of pearlite is investigated by phase-field simulation. Strain is considered in terms of expansion/contraction during transformation and due to concentration gradients in austenite. It is demonstrated that due to the concentration dependence of the eigenstrain, an inhomogeneous stress distribution ahead of the transformation front enhances diffusion in the austenitic phase and reduces chemical supersaturation in both austenite and ferrite. The main result of the investigation is that transformation strain inhibits the cooperative growth mode of cementite and ferrite, as considered by the Zener–Hillert model, and provokes the salient growth of cementite needles ahead of the ferrite front, which we call ''staggered growth''. The predicted growth velocities give the right order of magnitude compared to the experiment and close the gap between theoretical models based on diffusion only, and experimental observations.

Keywords: Pearlitic steels; Phase transformation kinetics; Phase field models

1. Introduction

Pearlite transformation has been a challenge for theoretical modeling since the pioneering work of Zener and Hillert in the 1950s [1,2]: it has been clear since then that the proposed transformation mode, taking only diffusion in austenite into account, fails to explain the experimentally observed transformation rates by a factor of 10. On the other hand, the explanation of the role of the interfacial energy contribution in spacing selection was a big success, stimulating a burst of research on pattern formation in materials science [3–5]. It has also become clear that there are a number of additional effects influencing the formation of pearlite; these include diffusion in ferrite, concentration dependence of diffusion coefficients, grain boundary diffusion and stress–strain effects. Most of these were ruled out for various arguments, as can be found in the discussion in Refs. [6,2]. Only two effects are currently the subject of discussion: grain boundary diffusion and enhanced diffusion due to stress. Verhoeven and Pearson [7] treated the latter effect by an accelerated volume diffusion in austenite and calculated a transformation rate with a factor of 3–4 below the experimental value. Grain boundary diffusion may further increase this rate. However, given the fast diffusion of carbon in both austenite and ferrite, it is unlikely that diffusion in grain boundaries is significantly higher than in the bulk [8]. Hillert concluded that the experimental observations can only be fitted by his model if an artificially high diffusion coefficient is assumed [9]. In a recent ''reappraisal of kinetic data for the growth of pearlite'' [10], Whiting came to a similar conclusion, but proposed a more ''complex diffusion process, coupled with the operation of a ledge and interdiffusion mechanism'', to explain the experimental results. A detailed description of the ledge growth mechanism is given in Ref. [11]. Such a mechanism, however, cannot explain the speeding up of the transformation beyond the diffusional limit. It rather implies interface friction, which would lead to a finite interface mobility, as it is known from the mixed-mode models of the austenite to ferrite transformation. According to the data from Krielaard

* Corresponding author. Tel.: +49 241 8098000; fax: +49 241 38578.
E-mail address: I.Steinbach@access.rwth-aachen.de (I. Steinbach).

1359-6454/$30.00
doi:10.1016/j.actamat.2007.05.013

et al. [12], the velocity of the ferrite and austenite interface should be significantly slowed down by interfacial friction, which additionally enlarges the gap between theory and experiment (see also the discussion in Ref. [7]).

It was in this context that we began to reconsider the effect of diffusion in ferrite by phase-field simulation [13]. The main result of this study was that diffusion in ferrite can considerably increase the transformation rate, as predicted by Fisher [14], but cannot fully close the gap to experimental findings. Moreover, the question remains that this transformation mode results in a conical growth shape of the cementite tip pointing towards the transformation front and thickening by transformation from the ferrite, a feature that has never been observed experimentally [6].

In the present work we examine the effect of stress and strain on the growth mode and the transformation kinetics of pearlite in a binary Fe–C alloy. We use the multi-phase-field method [15–17] and accomplish the stress–strain calculation by a concentration-dependent eigen-strain with an additional diffusive flux due to a gradient in hydrostatic stress. Using this model allows us to treat simultaneously all important effects mentioned above, including finite interface mobility. Grain boundary diffusion is, however, neglected in this study because of the lack of reliable materials data. The effects of plasticity and grain boundary gliding were also excluded. Furthermore, we do not attempt to resolve details of atomistic growth mechanisms, but treat the interface motion like that of a smooth front, governed by the balance of curvature, diffusion and mechanical equilibrium as described by the phase-field method in the Gibbs–Thomson limit. In this respect the work is a direct extension of Hillert's modeling approach [2].

In the following section the coupling of stress and diffusion in the framework of our phase-field model is briefly explained . Section 3 gives the simulation conditions and results. A new growth mode is proposed where cementite platelets precede the ferrite front, which has the potential to explain the experimental results. We call this mode "staggered growth". In the final section the results are discussed against the historical background. Some arguments are presented as to why the staggered growth mode can hardly be observed from a quenched transformation front and how an indirect verification of this transformation mode could be performed.

2. Phase-field model and materials data

The phase-field theory describes the evolution of so-called "phase fields" $\Phi_\alpha(\vec{x},t), \alpha = 1,\ldots,N$ for N different phases or grains. For pearlite, we treat the three different phases, austenite, ferrite and cementite, where ferrite or cementite lamellae, differing in orientation, will be assigned with separate phase fields ($cementite_1$, $cementite_2$, …, $ferrite_1$, $ferrite_2$, …). If the respective phase or lamella α exists locally $\Phi_\alpha = 1$, otherwise $\Phi_\alpha = 0$. At the interfaces the phase-field variable changes continuously from 1 to 0. Thus the interfaces have a thickness η, which can be selected to be large compared to the atomic interface thickness but small compared to the microstructural length scale. The equations of motion for the phase-fields Φ_α, concentration c and strain tensor ϵ^{ij} are (for details, see Ref. [16]):

$$\dot{\Phi}_\alpha = \sum_\beta \mu_{\alpha\beta}(\vec{n})\left[\sigma^*_{\alpha\beta}(\vec{n})K_{\alpha\beta} + \frac{\pi}{\eta}\sqrt{\Phi_\alpha\Phi_\beta}(\Delta G^{\mathrm{CH}}_{\alpha\beta} + \Delta G^{\mathrm{EL}}_{\alpha\beta})\right] \quad (1)$$

$$\dot{c} = \nabla^i \sum_{\alpha=1}^{N} \Phi_\alpha (D_\alpha \nabla^i c_\alpha - \nabla^i M_\alpha (\epsilon^1_\alpha)^{kl} s^{kl}) \quad (2)$$

$$0^i = \nabla^j \sum_{\alpha=1}^{N} \Phi_\alpha C^{ijkl}_\alpha (\epsilon_\alpha - (\epsilon^0_\alpha)^{kl} - c_\alpha (\epsilon^1_\alpha)^{kl}) \quad (3)$$

In Eq. (1), $\mu_{\alpha\beta}$ is the mobility of the interface as a function of the interface orientation $\vec{n}$. $\sigma^*_{\alpha\beta}$ is the interface stiffness, $K_{\alpha\beta} = \Phi_\alpha\nabla^2\Phi_\beta - \Phi_\beta\nabla^2\Phi_\alpha + \frac{\pi^2}{\eta^2}(\Phi_\alpha - \Phi_\beta)$ is the generalized curvature operator of the interface, $\Delta G^{\mathrm{CH}}_{\alpha\beta} = -f_\alpha(\vec{c}_\alpha) + f_\beta(\vec{c}_\beta) + \vec{\mu}(\vec{c}_\alpha - \vec{c}_\beta)$, with the chemical free energy of the related phases f_α and the chemical potential μ, is the chemical driving force of the interface $\alpha\beta$, and finally $\Delta G^{\mathrm{EL}}_{\alpha\beta} = s^{ij}((\epsilon^*_\alpha)^{ij} - (\epsilon^*_\beta)^{ij})$. The eigen-strain $(\epsilon^*_\alpha)^{ij} = (\epsilon^0_\alpha)^{ij} + c_\alpha(\epsilon^1_\alpha)^{ij}$ is concentration dependent in Vegard's approximation. $s^{ij} = s^{ij}_\alpha = (\epsilon^{kl}_\alpha - (\epsilon^*_\alpha)^{kl})C^{ijkl}_\alpha$ is the stress tensor, equal in all phases, with the total strain ϵ^{kl}_α per phase and the elasticity tensor C^{ijkl}_α. The sum convention for double indices i is used. The concentration c is a mixture of the phase concentrations c_α by $c = \sum_{\alpha=1}^{N}\Phi_\alpha c_\alpha$. D_α is the diffusion coefficient and M_α the chemical mobility in phase α, where both quantities are connected by Darken's law $D_\alpha = \frac{\delta^2 f_\alpha}{\delta c^2}M_\alpha$. Due to the dependence of eigenstrain on concentration, the second term in the concentration equation (Eq. (2)) accounts for diffusion due to stress inhomogeneity. The stress–strain equation (Eq. (3)) is treated in the quasi-static limit. All three equations are closely interrelated as each equation contains coupling terms to both of the other equations.

The thermophysical data used in the simulation are listed in Table 1. Phase diagram data were taken from a linearization of the binary Fe–C phase diagram around the eutectoid composition and temperature. The diffusion coefficient is temperature dependent, but an explicit composition dependence has been neglected, as it is treated implicitly by the stress contribution in the diffusion equation. The chemical mobility in the diffusion equation was assumed to be constant. Elastic material parameters were set identical for all phases and independent of temperature and composition. The composition dependence of the eigenstrain was only considered for austenite. The anisotropy of the eigenstrain of cementite was modeled in a two-dimensional (2-D) approximation, in such a way that the short axis (parallel to the direction of the lamella structure) matches the eigenstrain of ferrite, in order to construct a special grain boundary of low energy, as known for this interface [18]. The long direction was adjusted to match the molar volume of the cementite lattice. All grain boundary energies and mobilities were assumed to be isotropic, except in the simulation including transformation strain, where the cementite–austenite interface was

Table 1
Materials data used in the phase-field calculations

Interfaces	Interface energy	All	1.0 J m^{-2}
	Interface mobility	γ/α	5.0×10^{-5}– 1.0×10^{-4} cm^4 J^{-1} s^{-1}
			9.0×10^{-5}– 2.0×10^{-4} cm^4 J^{-1} s^{-1}
			9.0×10^{-8}– 5.0×10^{-7} cm^4 J^{-1} s^{-1}
Diffusion	Carbon	γ	$D_0 = 1.5\times10^{-1}$ cm^2 s^{-1}, $Q = 142.1$ kJ mol^{-1}
		α	$D_0 = 2.2$ cm^2 s^{-1}, $Q = 122.5$ kJ mol^{-1}
		Cem	Stoichiometric
	Chemical mobility	γ	5.0×10^{-12} cm^5 J^{-1} s^{-1}
Stress–strain	Elasticity modulus	All	208 GPa
	Poisson ratio	All	0.3
	Volume per substitutional atom	γ	0.0493 nm^3
		α	0.0489 nm^3
		Cem	0.0521 nm^3
	Expansion coeff. ε^1	γ	0.002151/%

modeled with a reduced interface stiffness in the growth direction to allow needle-like growth.

3. Simulation conditions and results

All simulations start from austenite with eutectoid composition of 3.446 at.% C at uniform and constant temperature, with a fixed undercooling below the eutectoid temperature of 997 K. A seed structure of ferrite and cementite with fixed spacing is set at the bottom of the calculation domain. The right and left boundaries of the rectangular 2-D domain were set as periodic for concentration and phase-field. The top and bottom boundaries were set as adiabatic for the phase-field. The bottom boundary was set as adiabatic for concentration, while the top boundary was treated with a 1-D extension for concentration, i.e., the concentration of the top layer is averaged and the far field diffusion is solved in a 1-D domain, large enough to resolve the diffusion pile up ahead of the pearlitic front. For the stress–strain calculation, approximated in 2-D by the plain strain condition, the domain was set to expand freely during transformation but retaining its rectangular shape. The calculations were executed by the software MICRESS [19].

Fig. 1 shows a series of calculations in which only diffusion in austenite (but no stress) was taken into account. This type of calculations was used to check the results against the classical Zener–Hillert theory and to investigate spacing selection according to the maximum growth hypothesis (for more details, see Ref. [13]). As discussed in Ref. [13] diffusion in ferrite increases the transformation rate by a factor of four. This is mainly due to reduced supersaturation of austenite.

Including concentration-dependent eigenstrain causes a region of compressive stress in front of the growing ferrite, where the austenite is supersaturated, and a region of tensile stress in front of the growing cementite, where the austenite is depleted of carbon. The stress distribution and corresponding carbon distribution is shown in Fig. 2. For the given conditions and 30 K undercooling, we calculate a maximum hydrostatic stress of 30 MPa in austenite directly in front of the cementite tip. Comparison of the concentration profiles from two calculations neglecting or including composition-dependent eigenstrain again shows a reduction in the supersaturation of austenite due to the effect of stress-driven diffusion. The lower concentration gradient in the case that includes concentration-dependent strain suggests a reduced transport of carbon through austenite. However, it can be calculated from the concentration and stress gradient in front of the cementite that stress-driven diffusion approximately equals chemical diffusion and that both fluxes together match the flux in the case

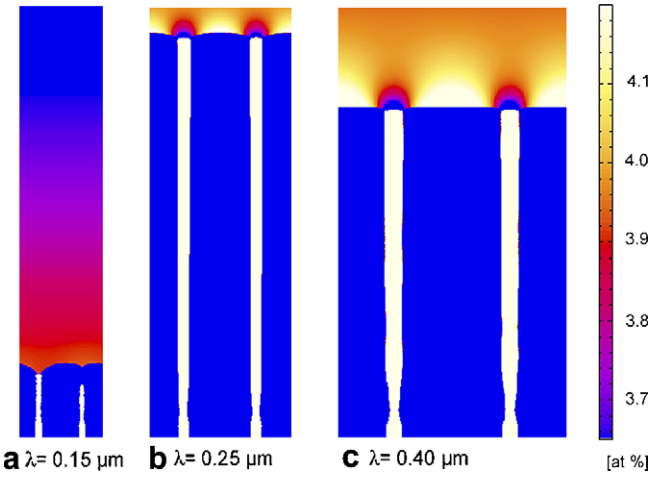

Fig. 1. Selection of optimal spacing for pearlite formation, taking into account only diffusion in austenite . The growth starts from seeds of ferrite and cementite at the bottom of the calculation domain. The lamella spacing is fixed by the calculation domain. (a) $\lambda = 0.15$ µm. The spacing is too small and stable growth cannot be established. (b) $\lambda = 0.25$ µm. Optimal spacing with maximum growth velocity. (c) $\lambda = 0.4$ µm. Spacing is too wide and growth velocity decreases. All calculations are shown at the same time after seeding. The color table denotes the carbon concentration. (For interpretation of color in this Figure, the reader is referred to the web version of this article.)

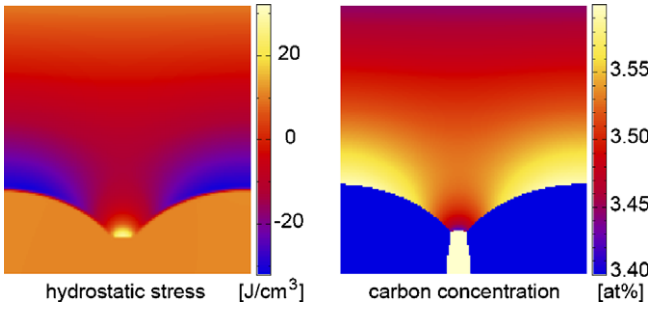

Fig. 2. Snapshot of the transformation region ahead of one cementite lamella. Left: Hydrostatic stress. The austenite in direct contact with cementite is under moderate tension due to the depletion of carbon. The supersaturated austenite in front of the ferrite is under compression. Right: Carbon profile. The carbon distribution is similar to the case without stress coupling.

in which only chemical diffusion is considered. As a result of the reduced supersaturation of the austenite in front of the ferrite, the transformation is accelerated again by a factor of roughly two. We deduce that supersaturation of austenite is the rate-controlling mechanism of the transformation, and that the carbon fluxes, which are required to fulfill the mass balance between ferrite and cementite, predominantly pass through the ferrite.

Including transformation strain completely alters the picture. The cooperative growth mode is no longer stable, because the high torsional forces caused by the transformation strain destabilize the triple junction. As long as the cementite interface is treated with an isotropic interfacial energy, no stable growth solution could be found. Inspired from observations of a needle-like growth of cementite [18], we applied a faceted model to the cementite–austenite interface: the interface is modeled with a cusp-like mobility, where the minimum lies 45° to the growth direction [20], and a cusp-like surface stiffness that is minimum in the direction of growth. The minimum mobility and surface stiffness were both set to 0.1 of the value of the isotropic interface. The reduction of the interface stiffness in the direction of growth corresponds to forbidden angles in the anisotropic Wulff shape of an interface that will evolve sharp edges or corners. The calculations now show a sharp cementite needle preceding into the austenite ahead of the austenite–ferrite front. Fig. 3 shows the result of the respective calculation. Starting from a situation similar to cooperative growth, after a short incubation time, a sharp cementite needle advances into the austenite ahead of the austenite–ferrite front. The needle in the 2-D simulation corresponds to a platelet in 3-D. Although the resolution of the calculation is rather poor, and it did not reach steady state because of computational restrictions, we found by variation of the parameters that the growth mode with the advancing cementite needle is a robust result that depends neither on the exact value of the interface stiffness nor on its mobility. The principal mechanism is an overall reduction of the curvature contribution to the driving force of the cementite–austenite interface that now allows a needle-like growth favored by the mechanical conditions. The diffusion fluxes coupled to the mechanical situation are sketched in Fig. 4. Due to the volume expansion related to austenite transformation into cementite, high tensile strain forms around the tip of the cementite platelet. Carbon diffuses into that region to fill the expanded lattice. The high carbon content of austenite around the cementite platelet now favors the transformation to cementite. The opposite happens in austenite in front of the ferrite: due to contraction of the austenite lattice when transforming to ferrite, this region becomes compressed. Compression favors diffusion of carbon away from ferrite. The austenite is locally depleted of carbon and transformation into cementite is favored compared to the diffusional growth mode. The carbon flux induced by the stress gradient (the second term on the right-hand side of Eq. (2)) is larger than the flux due to composition gradients. Close to the cementite tip, carbon diffuses uphill against the concentration gradient. On the other hand, the carbon supersaturation relaxes the elastic stress in this region considerably, so that a high volume expansion can be reached without leaving the elastic regime. Cementite growth from the supersaturated austenite is then very favorable and fast. From the simulation we evaluate a growth speed of $7\,\frac{\mu m}{s}$ for an undercooling of 30 K, which is exactly the magnitude for the transformation speed found experimentally. Fig. 5 compares transformation speed versus undercooling as predicted from the Zener–Hillert theory with phase-field calculations and data from experiments. Although the

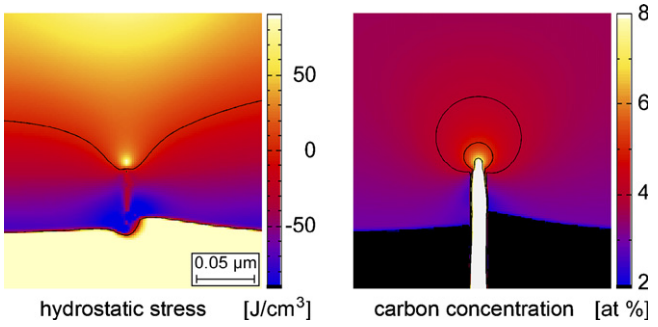

Fig. 3. Snapshot of the tip region as calculated for the staggered growth mode. Left: Hydrostatic stress. The austenite around the cementite tip is under large expansion, caused by the lattice match to cementite. A large part of the expansion is compensated by enrichment of carbon. Therefore elastic stress is limited to 90 MPa. The iso-line divides compressive (middle) from tensile stress. Right: Carbon distribution around the cementite tip. The carbon enrichment is mainly due to the expansion of the austenite lattice. The concentration reaches its maximum at 6 at.% in austenite.

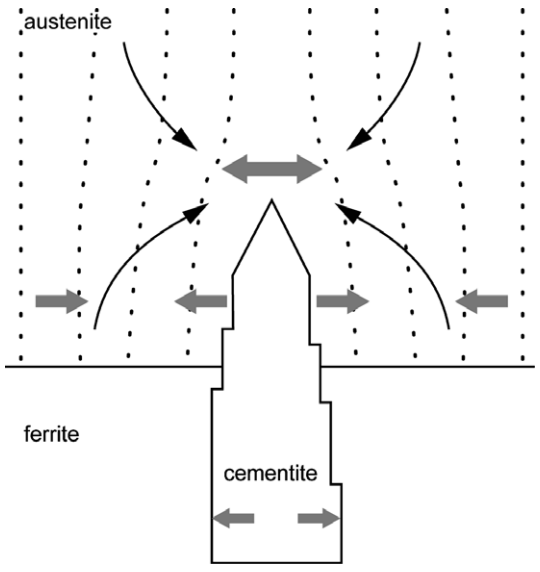

Fig. 4. Schematic picture of the staggered growth mode. The large molar volume of cementite promotes positive strain and tensile stress in austenite around the tip of the cementite platelet. Between the platelets austenite is under negative strain and compressive stress. Correspondingly carbon is forced to diffuse away from the austenite ferrite interface towards the tip of the cementite platelet.

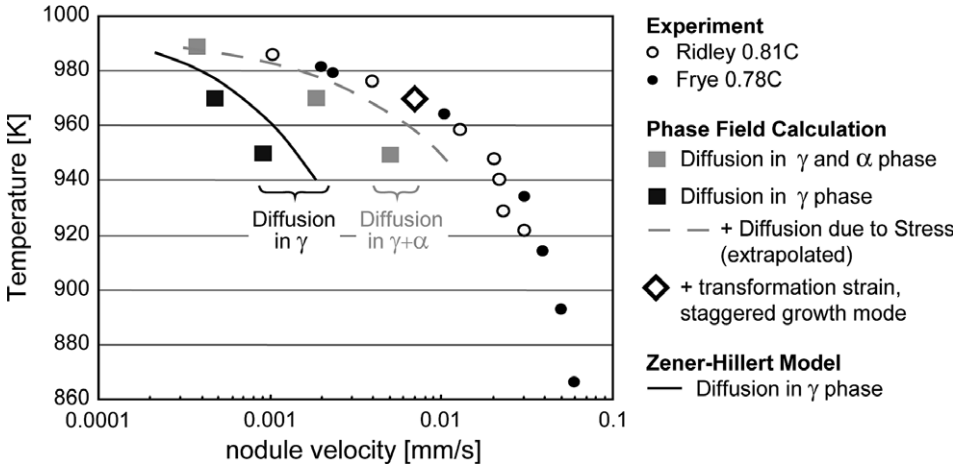

Fig. 5. Comparison of the growth rate of pearlite versus temperature (undercooling) between the Zener–Hillert model, phase-field simulations and experiment [27,28].

exact values of transformation speed deduced from the phase-field calculations are, due to computational limitations, associated with numerical uncertainties, we may conclude that all the various mechanisms discussed contribute to the transformation process and are required to explain the experimental observations. These various mechanisms are: (i) diffusion in both austenite and ferrite, (ii) concentration-dependent eigenstrain of austenite and stress-driven diffusion, (iii) transformation strain and (iv) platelet-like growth of cementite into austenite. Grain boundary diffusion will also contribute to the overall picture, as will finite interface mobility.

4. Discussion

Our phase-field simulations lead to the conclusion that the coupled growth mode of pearlite is unstable under the action of transformation strain. Instead a staggered growth mode becomes possible, which leads to the same lamellar eutectoid microstructure: cementite platelets grow into the austenite, followed by the ferrite within a distance comparable to the width of the cementite lamellae. This transformation mode may not be a new finding, since the pearlite transformation has been the object of scientific investigation for almost 100 years, and much of the original research may be not known to us. Some indications can be read from the paper of Mehl and Hagel [6], in which they report the experimental observation "indeed Fe_3C platelets often extend separately into the parent austenite" (p. 120), but the corresponding figure in their paper is not sufficiently conclusive in the sense that it could be interpreted as a proof of the existence of the staggered growth mode. Moreover the question remains how the structure of the front changes during quenching. Here we may note that cementite is a stoichiometric phase in terms of carbon and its growth is closely connected to the flux of carbon. During cooling, the lamellar spacing has to accommodate the shorter diffusion distances, which is not possible during a fast quench [21]. Therefore the cementite can not speed up during quench and ceases to grow if the carbon diffusion slows down at lower temperatures. Ferrite, on the other hand, will speed up and grow with increasing supersaturation until the interface mobility becomes too small or the austenite transforms to martensite. Certainly ferrite will grow up to the cementite tip, where austenite is depleted from carbon. Eventually it will overgrow the cementite needles/platelets. This is the picture that is commonly reported from quenched pearlite structures and can be reconciled with the proposed staggered growth mode. As a consequence, there should be a larger number of precipitated carbides in the zone, where ferrite has grown during the quench, than in the zone grown under constant conditions. This increase in carbide precipitation should be detectable experimentally and could be used as an indirect proof of the proposed growth mode.

Our observation, that in pearlitic Fe–C the cooperative growth mode is unstable should not be interpreted as disproving this growth mode in general or the existence of this growth mode in other eutectoid systems (see e.g. Refs. [22,23]). In fact the staggered growth mode develops from the cooperative growth mode under certain circumstances, as described for Fe–C, in particular the strong dependence of austenite volume on carbon content. Therefore the staggered growth mode may not be existent in other materials, where cooperative growth is stable. We should also compare the proposed growth mode with the ledge-wise growth mode proposed by Shiflet and co-workers [24,11]. They present experimental evidence that growth ledges proceed over several lamella of cementite and ferrite. Hence the growth front motion should be dominated by ledge growth, which also can explain orientation relationships between the pearlitic phases (see e.g. Ref. [25]). This should not, however, be misinterpreted as a contradiction to the staggered growth mode, as in any case the ledges have to be transferred from one lamella to the next at the triple junction. Also, the same diffusional fluxes are necessary to explain the observed growth kinetics of pearlite if ledge-wise growth is considered or not. In this sense, growth

ledges will determine the exact interface structure on the atomistic scale, which is not resolved in our calculations, but they will not contribute to the diffusional fluxes on the mesoscopic scale of the lamellar structure.

A further aspect is the role of carbon diffusion in ferrite. This diffusion mode should enhance the transformation kinetics as proposed by Fisher [14] and Onsager [26], as cited by Mehl and Hagel [6], and recalculated by ourselves [13]. Because of the lack of experimental evidence of cementite growing from the ferrite, this growth mode was rejected by Mehl and Hagel [6]. In the staggered growth mode, diffusion in ferrite might be far less important than in coupled growth. In the staggered growth mode, a large fraction of cementite grows directly from the austenite and no wedge-shaped cementite lamellae will be formed.

Our calculation results are – because of computational limitations – not detailed enough to allow a quantitative separation of the various growth contributions; however, they give a strong argument that staggered growth enables faster transformation than the cooperative growth model without the need for fast grain boundary diffusion. We may therefore conclude that one should reconsider the old experiments in the light of the proposed model and that more detailed calculations and new experiments will be needed before a final decision can be made.

References

[1] Zener C. Kinetics of the decomposition of austenite. New York: Interscience/John Wiley; 1947.

[2] Hillert M. The role of interfacial energy during solid state phase transformations. Jerekont Ann 1957;147:757–89.

[3] Jackson KA, Hunt JD. Lamellar and rod eutectic growth. Trans Metall Soc AIME 1966;236:1129–42.

[4] Trivedi R. Growth of dendritic needles from a supercooled melt. Acta Met 1970;18:287.

[5] Han SH, Trivedi R. Primary spacing selection in directionally solidified alloys. Acta Met 1992;42:25–41.

[6] Mehl RF, Hagel WC. The austenite: Pearlite reaction. Prog Metal Phys 1956;6:74–134.

[7] Verhoeven JD, Pearson DD. Forced velocity pearlite in high purity fe-c alloys: Part ii. theoretical. Met Trans A 1984;15:1047–54.

[8] Hillert M. Private communication per e-mail, 2005.

[9] Hillert M. Review paper: Eutectoid transformation of austenite. In: Chemical metallurgy of iron and steel. London: The Iron Steel Institute; 1973. pp. 241–7.

[10] Whiting MJ. A reappraisal of kinetic data for the growth of pearlite in high purity Fe–C eutectoid alloys. Scripta Mat 2000;43:969–75.

[11] Zhou DS, Shiflet GJ. Interfacial steps and growth mechanism in ferrous pearlites. Met Trans A 1991(22):1349–65.

[12] Krielaard GP, Sietsma J, Van der Zwaag S. Ferrite formation in Fe–C alloys during austenite decomposition under non-equilibrium interface conditions. Mat Sci Eng A 1997;237(6):216–23.

[13] Nakajima K, Apel M, Steinbach I. The role of carbon diffusion in ferrite on the kinetics of cooperative growth of pearlite: A multi-phase field study. Acta Mat 2006;54:3665–72.

[14] Fisher JC. Themodynamics in physical metallurgy. Am Soc Metals Sem 1950:201.

[15] Steinbach I, Pezzolla F, Nestler B, Seeßelberg M, Prieler R, Schmitz GJ, et al. A phase field concept for multiphase systems. Physica D 1996;94:135–47.

[16] Steinbach I, Apel M. Multi phase field model for solid state transformation with elastic strain. Physica D 2006;217:153–60.

[17] Eiken J, Böttger B, Steinbach I. Multi phase field approach for alloy solidification. Phys Rev E 2006;73. 066122–1–9.

[18] Durand-Charre M. Microstructure of steels and cast iron. Springer; 2003. p. 197.

[19] <www.micress.de>.

[20] Steinbach I, Pezzolla F, Prieler R. Grain selection in faceted crystal growth using the phase field theory. In: Cross M, Campbell J, editors. Modelling of casting, welding and advanced solidification processes VII. TMS; 1995. p. 695–703.

[21] Hillert M. The formation of pearlite. In: Zackay VF, Aaronson HI, editors. Decomposition of austenite by diffusional processes. New York: Interscience/John Wiley; 1962. p. 197–248.

[22] Whiting MJ, Tsakiropoulos P. Morphological evolution of lamellar structures: The Cu–Al eutectoid. Acta Mat 1996;45:2027–42.

[23] Zelenitsas K, Tsakiropoulos P. Study of the role of Al and Cr additions in the microstructure of Nb–Ti–Si in situ composites. Intermetallics 2005(13):1079–95.

[24] Hackney SA, Shiflet GJ. The pearlite–austenite growth interface in an Fe-0.8 C-12 Mn alloy. Acta Met 1987;35:1007–17.

[25] Magnan MA, Shiflet GJ. The pitsch-pech orientation relationship in ferrous pearlite at small undercooling. Mat Trans A 1999;30:2767–81.

[26] Onsager L. Phase transformations in Solids, Conference, Cornell, Ithaca, NY. New York: Wiley; 1951. p. 37.

[27] Brown D, Ridley N. J Iron Steel Inst 1969;207:1232–40.

[28] Frye JH, Stansbury EE, McElroy DL. Trans AIME 1942;150:185–207.